RSC Advances

PAPER

View Article Online
View Journal | View Issue

Cite this: *RSC Adv.*, 2022, **12**, 33612

Light-driven autonomous swing of multi-layered hydrogel†

Shunsuke Nakamura, Momoka Yamanaka, Yushi Oishi and Takayuki Narita *

Received 11th September 2022
Accepted 17th November 2022

DOI: 10.1039/d2ra05722k

rsc.li/rsc-advances

Light-driven self-oscillators without electronic circuits or conventional heat engines are carbon-emission-free systems and hold promise for developing autonomous transmission pumps and self-swimming micromotors. Thermosensitive hydrogels as self-oscillators can be used in the exploitation of low-temperature heat sources and in medical applications since the driving temperature is close to body temperature. Here, the autonomous swinging of the hydrogel was achieved by irradiating a constant light beam onto a head laminated with two thermosensitive hydrogels with different transition temperatures. Hysteresis resulting from the transition point difference between the two hydrogels allowed the light-driven self-oscillation without self-shadowing from the irradiation. The proposed theoretical model and numerical simulations explain this light-driven continuous swing, and the results agree qualitatively well with the experiments.

In living organisms, rhythmic activities such as ionic changes inside cells, cardiac pumping, and metabolism sustain their lives.[1] For example, our heart pumps and circulates blood through a rhythmical chemical oscillation.[2] Studying novel rhythmic materials mimicking such natural processes is meaningful for understanding living systems and device developments to achieve high-efficiency energy conversion and production observed in living organisms. Artificial pumps mimicking heartbeats have considerable promise as innovative liquid pumps using non-electric energy.[3–5] Such notable self-oscillators of soft materials have been intensely studied.[5–16] For example, Yoshida and co-workers have reported novel liquid pumps using self-oscillating gel,[6] which combine a thermosensitive hydrogel and a Belousov–Zhabotinsky (BZ) reaction, chemical oscillation.[7] These soft self-oscillators are driven by chemical energies: chemical potentials generated by chemical reactions are converted to kinetic energy (volumetric work) through osmotic pressure differences inside and outside the compartment. Since chemical reactions drive their self-oscillators, they require continuous chemical supplies to maintain the activity. This fact means that their activity reaches an arrested state sooner or later for thermodynamically closed systems, in which energy transfers to the surrounding environment across the material. Rhythmic activities workable even in closed systems then will be very attractive for expanding the oscillator's applications into self-propelling pumps and motors available even in environments where material supplies are difficult like outer space and the interior of our body; this is because oscillating motions have been widely used in primary mechanisms in typical pumps and motors. In closed systems, light is an available energy source for supply; sunlight is an easily accessible and carbon-emission-free resource.

Some light-driven self-oscillators have recently developed, which can oscillate rhythmically using stationary light.[9–16] These soft oscillators are achieved mainly using photoactive liquid crystal polymer films[9–12] or polymer gels as the main component.[14–16] As the polymer gel-based light-driven oscillators, evaporation-driven oscillator utilising solvent vapour generated by light-thermal conversion in the gel has been reported.[14,15] Other gel-based photo-driven oscillators employ a volume phase transition for their deformation. These light-driven oscillators have embedded photothermal conversion materials inside these gels. In principle, volume phase transition-based oscillation systems can be driven at temperatures as low as or lower than body temperature. Thus, they offer the potential for medical applications and novel light energy harvesting devices.

Previous light-driven self-driven soft oscillator materials listed have been activated by a feedback loop through self-shadowing a part of themselves of the deformed material caused by light acceptance hides the light-receiving part. In this case, the light must be intercepted by the deformed part, which must target a middle part of the material. In this case, the deformed part must intercept the light by itself, resulting in light irradiation on a middle part of the material.

Here we propose a new light-driven hydrogel self-oscillator utilising the concept of hysteresis, which does not require shielding itself from light. Many natural biological oscillating

Department of Chemistry and Applied Chemistry, Saga University, 1 Honjo, Saga 840-8502, Japan. E-mail: naritat@cc.saga-u.ac.jp; Fax: +81 952-28-8805; Tel: +81 952-28-8805

† Electronic supplementary information (ESI) available: Experimental details, supporting Video S1–S4, additional Fig. S1–S4. See DOI: https://doi.org/10.1039/d2ra05722k

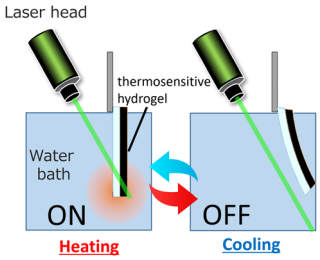

Fig. 1 Schematic diagrams illustrating the concept of the self-propelled swing driven by a stationary laser radiation.

systems use hysteresis to achieve stable periodic behaviour. Hysteresis is a difference in the phase transformation temperatures between cooling and heating.[17–19] However, no pulsation has been observed when light is irradiated on typical photo-responsive hydrogels with hysteresis at the transition point.[20] To bring a rhythmic motion to the light-driven hydrogel system, we investigated the introduction of macroscopic deformation and two different transition points. A large deformative hydrogel, which is light-driven, has been demonstrated by Lee, E. *et al.* using double-layered gels composed of thermosensitive polymers; it deforms to a crescent shape by light irradiation.[21] Because such large deformation self-modifies the light-receiving area by the gel shrinking, we used a multi-layered thermosensitive gel containing two lower critical solution temperatures (LSCT) to design the hysteresis effect. The system is inspired by bimetallic thermostat systems (see Fig. 1), which warms and bends the light-irradiated gel head to promote its release from the laser beam path. In contrast, the non-light-receiving gel head cools and hangs straight down, resulting in re-hitting the laser spontaneously. Such a gel system then selfly switches the laser receiving and passing states by repeating the heating driven by light receive and the cooling by heat release.

The volume phase transition temperatures (PTT) of the single-layer PNIPAm and PNIPAm-co-AAm gels were determined by the temperature dependence of the swelling ratio for each layer gel, which was 33 °C and 41 °C, respectively (see Fig. S1†). The gel multilayer bar used consisted of an upper PNIPAm transparent layer, a middle black AAm phase, and a lower white PNIPAm-co-AAm layer (see Fig. 2(a) and (b)). The PNIPAm gel in the upper layer was cut in half, resulting in an asymmetrical rod like a toothbrush. The bar end in the three-layer gel with a PNIPAm layer has been designated the "gel head." The opposite end without the PNIPAm layer has been termed the "gel tail". Fig. 2(c) shows a laser-irradiated image of the gel head suspended in a temperature-controlled cell filled with distilled water. The head of the gel bar swings continuously under steady-state laser beam irradiation, as shown in Fig. 2(d) and Video S1.† The irradiated gel head continuously swung back and forth at regular intervals from 300 to 600 s during the laser irradiation.

Fig. 2(e)–(g) shows the time course of the positions $X(t)$ of the hydrogel head in the lateral axis (moving forward for the irradiated spot is the positive direction) at different ambient temperatures T_{base}; Fig. 2(e) and Video S2† show the results at T_{base} = 10 °C, Fig. 2(f) and Video S3† are at T_{base} = 20 °C, and Fig. 2(g)

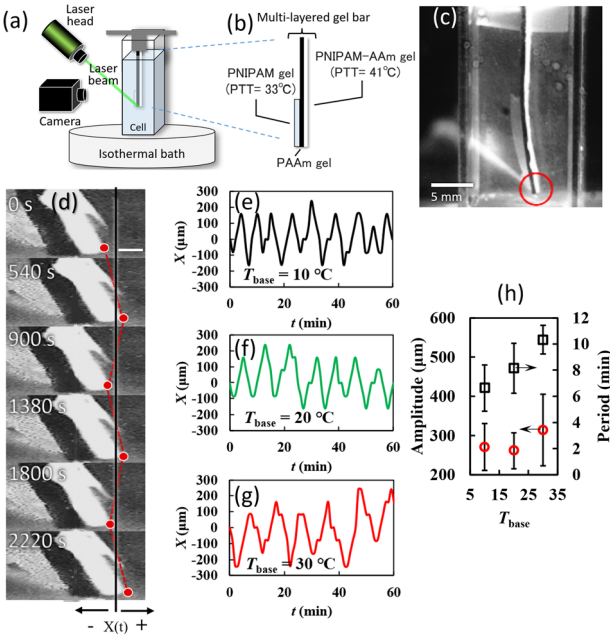

Fig. 2 The gel head motions of the multi-layered gel when a green laser irradiated the gel. (a) Schematic diagram of laser irradiation apparatus for the multi-layered gel and (b) the composition of the layered gel. (c) The overall image of the irradiated multi-layered gel. (b) Time sequential magnified images of the swing motion of the irradiated gel head. The arrows under the fig represent the swing directions. The white bar represents 1 mm. (e)–(g) Time courses of the swing head position $X(t)$ observed experimentally at the indicated ambient temperatures of (e) 10 °C, (f) 20 °C, and (g) 10 °C. (h) Experimental amplitudes and periods were obtained from the periodic motion at each ambient temperature T_{base}.

and Video S4† are at T_{base} = 30 °C. These time evolution curves can be approximated as a sine waveform. The specific periods can be 6.6 ± 1.8 min, 8.1 ± 1.9 min, and 10.3 ± 1.1 min at the water cell's temperature of 10, 20, 30 °C, respectively. The amplitudes were 271 ± 60, 261 ± 45.9, and 314 ± 91 μm for these temperatures, respectively. Fig. 2(h) shows the temperature dependence of the amplitudes and the periods extracted from the sinusoidal curves of the time evolution of $X(t)$. These results reveal that the system depends on the ambient temperature; the swing period and the amplitude increase with the ambient temperature.

Based on the design of this system, we consider the scenario of the self-propelling swinging, as illustrated in Fig. 3. Receiving the laser beam on the gel head firstly warms the gel by the light-heat exchange of the black-coloured gel (PAAm gel). Upon reaching the gel temperature of 33 °C (transition temperature of PNIPAm gel), the left gel (PNIPAm) layer shrinks, moving the gel head in the negative direction (Fig. 3(i)). Reaching 41 °C (PTT of PNIPAm-co-AAm gel) by the laser heating, the right side of the gel (PNIPAm-co-AAm gel, backside PNIPAm layer) contracts, and the gel head bends toward the positive direction (Fig. 3(ii)). The laser beam heats the gel until the gel releases the laser pass from the head. A significant positive bend should release the gel head from the laser pass, as this system is designed as a positive bend overcomes the negative one (Fig. 3(iii)). The laser detaches from the gel head and cools the gel bar by heat release to the

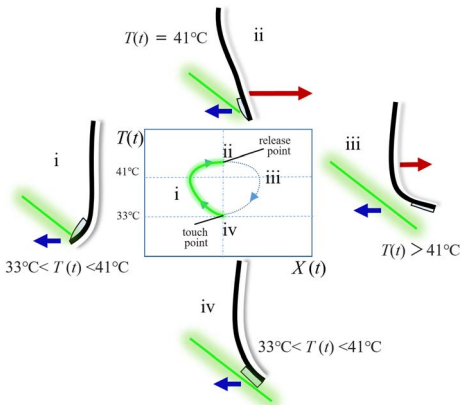

Fig. 3 Schematic representation of the preferred shapes and the process of the gel bar at various temperature regimes. The red arrows show the applied force given by the PNIPAm gel layer. The blue arrows are that by the PNIPAm-co-AAm gel layer. The graph inside the diagram represents the lateral head position $X(t)$ at the gel temperature $T(t)$. The green part in the cycled curve represents the predicted sections that the gel head catches the laser beam.

environment, resulting in the gel head returning to the start point and re-starting to receive the laser beam (Fig. 3(iv)). Because the PTTs differ between the PNIPAm gel and the PNIPAm-co-AAm gel, the light-receiving temperature between the start and end should be different; this difference is a temperature hysteresis at the same position, $X(t)$.

The thermodynamic state of the multilayer hydrogel in this study is most simply described by two parameters: the gel temperature $T(t)$ and the gel head position $X(t)$. The time derivative of the position, $dX(t)/dt$, could change by two driving forces related to the deformation of the multi-layered gel. One of the forces is the shrinking of the PNIPAm gel. Another is that of PNIPAm-co-AAm gel. The time derivative $dX(t)/dt$ is positive for the PNIPAm-co-AAm gel shrinking (right bend), in contrast, and is negative for the PNIPAm gel shrinking (left bend). The kinetics of the phase transition of thermosensitive gels can be described as a single exponential function given by the Tanaka–Fillmore theory.[22] Hence, $dX(t)/dt$ is linear with the difference between the equilibrium positions and $X(t)$ at time t.[23] The equilibrium positions of both gels can be set to $X = 0$ in the swollen states at temperatures below the phase transition ($T(t) < T_{trans}$). In the shrunk state, the equilibrium points are X_{NIsh} and X_{AAsh} for PNIPAm and PNIPAm-co-AAm gel, respectively. X_{NIsh} is a negative value due to the PNIPAm gel bending negatively, and X_{AAsh} is positive as the PNIPAm-co-AAm gel bends positively. The absolute value of X_{NIsh} is smaller than X_{AAsh} because PNIPAm gel has half the area of PNIPAm-co-AAm gel, leading to poor shrinkage and bending. Thus, the time evolution equation for the head position, $X(t)$, is most simply given by

$$\frac{d}{dt}X(t) = k_1\left(\left(\begin{cases} 0 & T(t) < T_{NItrans} \\ X_{NIsh} & T(t) \geq T_{NItrans} \end{cases}\right) - X(t)\right) + k_2\left(\left(\begin{cases} 0 & T(t) < T_{AAtrans} \\ X_{AAsh} & T(t) \geq T_{AAtrans} \end{cases}\right) - X(t)\right) \quad (1)$$

where k_1 and k_2 are positive constants. The first term of this equation accounts for the force contribution to the minus direction caused by the shrinking of the PNIPAm gel. The second is the contribution toward the plus-direction by PNIPAm-co-AAm (right side layer). As mentioned above, this system is purposely designed to enable the PNIPAm-co-AAm gel's shrinking force to overcome PNIPAm above the PNIPAm-co-AAm gel's PTT; the gel bar bends in the positive direction at gel temperatures higher than 41 °C. The difference in the PTTs of the PNIPAm and PMIPAM-AAm gels avoids the cancellation of opposing forces on the gel head. This cancellation allows the gel head to swing smoothly in the negative direction above the PNIPAm transition point and the positive direction above the PNIPAm-co-AAm transition point.

While, the time derivative of the gel temperature ($dT(t)/dt$) can be expressed in terms of heating contributed by the laser receiving and cooling from the heat release to the environment controlled by setting the temperature of the water bath T_{base}. The heating rate will be constant if the black gel (PAAm gel) is exposed to the laser due to the photothermal conversion at the PAAm gel layer. In contrast, excessive bending of the gel in the positive direction moves the head away from the laser beam path; the heating rate goes to zero. We thus assumed that below $X(t) = 0$, the gel is heated by the laser light ($dT/dt > 0$), but at $X(t) > 0$, it is no longer heated because the gel receives no laser light ($dT/dt = 0$). The cooling rate of the gel is proportional to the temperature difference between $T(t)$ and T_{base}. The time evolution equation of $T(t)$ is then given by the following:

$$\frac{d}{dt}T(t) = k_3\left(\begin{cases} 0 & X(t) > 0 \\ 1 & X(t) \leq 0 \end{cases}\right) - k_4(T(t) - T_{base}) \quad (2)$$

where k_3 and k_4 are positive constants. We numerically solved these coupled differential equations using the Runge–Kutta–Fehlberg fourth-fifth order method with the symbolic algebra software Maple.

Fig. 4(a)–(c) show the time course of calculated temperature $T(t)$ and position $X(t)$ at different ambient temperatures T_{base}; the parameters used are shown in the figure caption. We can see that $X(t)$ and $T(t)$ undergo periodic time evolutions from the data. Fig. 4(d) illustrates the calculated phase diagrams of $T(t)$ *vs.* $X(t)$ under the same condition as those in Fig. 4(a)–(c). As shown in the calculated diagram, the head positions of $X(t)$ take different values in the forward and backward paths at a given temperature between 33 °C and 70 °C. The simulation-based swing characteristics are qualitatively similar to the experimental ones in the 10 to 30 °C temperature range; both the swing amplitude and period are a positive function of the ambient temperature. This fact suggests that our numerical model reproduces well the experimental observations.

To confirm the importance of hysteresis, we exchanged the right-side transparent gel (PNIPAm gel) into NIPAm-AAm gel: both side gels were composed of the PNIPAm gel layer. The gel bar equipping PNIPAm gel on both sides displayed no automatic swing by the laser irradiation in the experiment (S5 Video†). To compare this experimental result by a calculation, we solved the differential equation using $T_{NItran} = T_{AAtran} = 41$. The

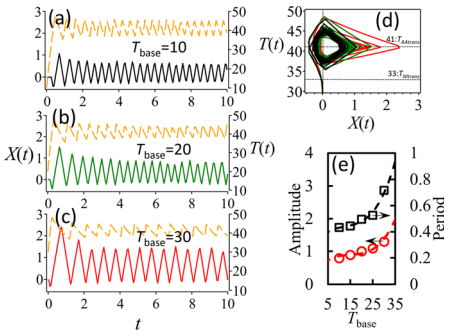

Fig. 4 The theoretical results obtained by numerically solving the differential equation system of eqn (1) and (2). The equations were solved by the given parameters of $k_1 = 0.1$, $k_2 = 0.1$, $k_3 = 100$, $k_4 = 1$, and $k_5 = 0.01$, $X_{NIsh} = -50$, $X_{AAsh} = 100$, $T_{NItrans} = 33$, $X_{AAtrans} = 41$. (a)–(c): The time courses of $X(t)$ (solid curve) and $T(t)$ (dashed curve) calculating as T_{base} = (a) 10, (b) 20, (c) 30. (d) The phase diagrams of $X(t)$ *vs.* $T(t)$ calculated in these T_{base}. The colours of the circle curves correspond to (a)–(c). (e) The calculated amplitudes and periods at each temperature T_{base}. The dashed curves are drawn as a guide for the eye.

converted the PTT of PNIPAm T_{NItran} with that of NIPAm-AAm gel T_{AAtran} saturates a constant value of $X(t)$ close to 0 after one cycle of swing (See Fig. S3(a)†). The results indicate that hysteresis based on the transition difference between PNIPAm and PNIPAm-AAm is fundamental for periodic motion.

Similarly, no multi-swing was observed by setting $X_{NIsh} = 0$ or $k_1 = 0$ on the first term of eqn (1), as shown in Fig. S3(b) and (c),† respectively. This non-continuous swing induced by the first-term elimination supports the idea that the back-to-back placement of gels with different PTTs allows the gel bar to swing continuously. Additionally, the gel failed to oscillate in the calculation when X_{AAsh} and X_{NIsh} were equal, as shown in Fig. S3(d)†: the contraction equilibrium points of PNIPAm and PNIPAm-co-AAm gel were the same in absolute value. The self-sustaining oscillations appeared in the calculation between $-100 < X_{NIsh} < -15$ at $X_{AAsh} = 100$ (see Fig. S4†). These calculations indicate that the asymmetry of contraction equilibrium values is essential for the continuous swing. This asymmetry of the shrinking equilibrium value modified the time evolution curve. This calculated swing amplitude had a maximum value when the shrinking equilibrium value of NIPAm was about half the value of PNIPAm-co-AAm ($X_{NItran} = 1/2\ X_{AAmtran}$) (see Fig. S4(e)†). The amplitude is small, especially when calculated with X_{NItran} close to the oscillation threshold. This reduced amplitude due to increased symmetry would explain why the swings are difficult to observe in experiments with symmetric gel bars having the same length of the NIPAm and PNIPAm-co-AAM gel layers.

Optical axis positioning would also be vital for this system. This is because the autonomous oscillation here requires transitioning from a high-to a low-efficiency light-to-heat conversion situation. This means that autonomous motion will not be triggered when light is irradiated to the areas where this transition does not happen. In oscillateable states, the irradiation spot position should be related to the gel head's initial position X_0 and the light-thermal conversion's linearity. The changes of initial position X_0 affect the amplitude and period values significantly in the early stage but finally reach the same values described above, according to the results of numerical simulations.

Our oscillation device consists of non-oriented gels. Thus, the irradiated light does not need to be polarized based on the mathematical model: it indicates that photothermal conversion is essential but polarization or not is little matter in thermal light conversion in our system.

In conclusion, this study designed a novel gel-rod continuous oscillation system driven by a steady light source. Our experimental and theoretical results successfully demonstrate that light-driven autonomous swing without self-shadowing effects can be accessed using a combination of thermo-responsive hydrogels with different transition temperatures. The three-layered gel bar with two different temperature-sensitive gels stuck against each back-to-back could swing continuously when the gel tip was irradiated with a steady-state laser beam. We also explained the oscillatory states using a mathematical model and reproduced the experimental cyclic swing. Notably, our experimental and simulation results demonstrate that the force asymmetry, the difference in PTTs, and the use of more than one gel contraction are key factors for the sustained laser swing of the gel through the volume phase transition.

These newly discovered insights will provide a way to build a novel pump that requires no electronic device using a steady-state light source, such as sunlight, and a possible artificial control tool. The simple strategy will expand the development potential of light-driven self-oscillating devices (light-driven engines), even if their efficiency is low today. The oscillation frequency obtained here is quite low and takes several minutes to complete one cycle. Hence, the current system is limited in its practical application. To bring enough force to transport the fluid, not only must the shape and optical axis be modified, but also to address the heat loss effects of liquid flow, while improving and optimizing the hydrogel's strength and robustness to handle fluid flows.

Conflicts of interest

There are no conflicts to declare.

Acknowledgements

The authors gratefully acknowledge financial support from JSPS (Japan Society for the Promotion of Science) Grant Number 18K05061.

Notes and references

1 L. Glass, *Nature*, 2001, **410**, 277–284.
2 G. Leon, C. Mackey Michael and F. Zweifel Paul, *From clocks to chaos In From Clocks to Chaos*, Princeton University Press, 1988.

3 H. Banerjee, M. Sivaperuman Kalairaj, H. Ren and A. Jusufi, *Adv. Eng. Mater.*, 2021, **23**, 2100121.
4 Y. Fang, W. Sun, T. Zhang and Z. Xiong, *Biomaterials*, 2022, **280**, 121298.
5 R. Merindol and A. Walther, *Chem. Soc. Rev.*, 2017, **46**, 5588–5619.
6 R. Yoshida, T. Takahashi, T. Yamaguchi and H. Ichijo, *J. Am. Chem. Soc.*, 1996, **118**, 5134–5135.
7 Y. Shiraki and R. Yoshida, *Angew. Chem.*, 2012, **124**, 6216–6220.
8 H. Zhou, X. Ding, Z. Zheng and Y. Peng, *Soft Matter*, 2013, **9**, 4956–4968.
9 S. Serak, N. Tabiryan, R. Vergara, T. J. White, R. A. Vaia and T. J. Bunning, *Soft Matter*, 2010, **6**, 779–783.
10 A. H. Gelebart, D. Jan Mulder, M. Varga, A. Konya, G. Vantomme, E. W. Meijer, R. L. B. Selinger and D. J. Broer, *Nature*, 2017, **546**, 632–636.
11 H. Zeng, M. Lahikainen, L. Liu, Z. Ahmed, O. M. Wani, M. Wang, H. Yang and A. Priimagi, *Nat. Commun.*, 2019, **10**, 1–9.
12 G. Vantomme, L. Elands, A. H. Gelebart, E. W. Meijer, A. Y. Pogromsky, H. Nijmeijer and D. J. Broer, *Nat. Mater.*, 2021, **20**, 1702–1706.
13 Z. Hu, Y. Li and J.-a. Lv, *Nat. Commun.*, 2021, **12**, 1–9.
14 Z. Li, N. V. Myung and Y. Yin, *Sci. Robot.*, 2021, **6**, eabi4523.
15 J. Li, L. Mou, Z. Liu, X. Zhou and Y. Chen, *Nat. Commun.*, 2022, **13**, 1–11.
16 Y. Zhao, C. Xuan, X. Qian, Y. Alsaid, M. Hua, L. Jin and X. He, *Sci. Robot.*, 2019, **4**, eaax7112.
17 K. R. Allakhverdiev, F. A. Mikailov, A. M. Kulibekov and N. Türetken, *Phase Transit.*, 1998, **67**, 457–465.
18 N. Ma, G. Song and H. J. Lee, *Smart Mater. Struct.*, 2004, **13**, 777.
19 Z. Biolek, D. Biolek and V. Biolkova, *Radioengineering*, 2013, **22**, 132–135.
20 S. Nakamura, S. Onimaru, Y. Oishi and T. Narita, *Polymer*, 2017, **116**, 534–539.
21 E. Lee, D. Kim, H. Kim and J. Yoon, *Sci. Rep.*, 2015, **5**, 1–8.
22 T. Tanaka, E. Sato, Y. Hirokawa, S. Hirotsu and J. Peetermans, *Phys. Rev. Lett.*, 1985, **55**, 2455.
23 T. Narita, T. Yamamoto, D. Suzuki and T. Dobashi, *Langmuir*, 2003, **19**, 4051–4054.